Electrolytic deposition of amorphous and crystalline zinc–calcium phosphates

P. T. OLESEN, T. STEENBERG, E. CHRISTENSEN, N. J. BJERRUM
Department of Chemistry, Building 207, Technical University of Denmark,
DK-2800 Lyngby, Denmark

Amorphous Zn–Ca phosphates and crystalline $Zn_3(PO_4)_2 \cdot 4H_2O$ conversion layers on cathode substrates were prepared by electrolysis of mixtures of acidic solutions saturated with metal phosphates. The solutions contained tricalcium phosphate ($Ca_3(PO_4)_2$) and/or zinc phosphate dihydrate ($Zn_3(PO_4)_2 \cdot 2H_2O$). The depositions was carried out with constant or pulsating cathode current densities in the range 20–70 mA cm^{-2} at 20–70 °C. The deposition of the uniform crystalline $Zn_3(PO_4)_2 \cdot 4H_2O$ was performed at a pulsating cathode current density of 70 mA cm^{-2} at 70 °C for periods up to 10 min. Amorphous deposits of Zn–Ca phosphates containing 20 wt% H_2O with variable Zn-to-Ca ratios were deposited at a constant cathodic current of 30 mA cm^{-2} at 20 °C for 3 min. Surface areas of the amorphous deposits were of the order of 28 m^2 g^{-1}. X-ray diffraction, differential thermal analysis and thermogravimetry were used to investigate phase *formation and transitions* at increasing temperatures. The amorphous Zn–Ca phosphate deposit was after calcination at 900 °C transformed to crystalline phosphates containing the β-$Ca_3(PO_4)_2$ or $Ca_{3-x}Zn_x(PO_4)_2$ and α-$CaZn_2(PO_4)$ phases. © *1998 Kluwer Academic Publishers*
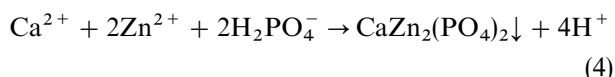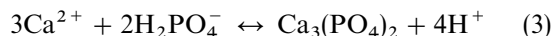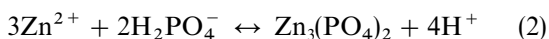
1. Introduction

Zinc and calcium phosphate conversion layers have been extensively studied because of their anticorrosion, biocompatible and lubrication properties. Depositions of zinc phosphate is used as a corrosion protection coating on low-alloy steel or zinc-plated steel. Crystalline zinc phosphate is deposited either by a chemical process or by an electrochemical process [1, 2]. Deposition of calcium phosphates is used as a biocompatible coating on implants. Calcium phosphate can be deposited by an electrochemical process [3–5].

The chemical phosphatizing of low-alloy steel takes place when the steel is immersed in a phosphatizing solution based on dilute nitric acid and phosphoric acid with one or more alkali-metal or heavy-metal ions. The solution contains essentially free phosphoric acid and orthophosphates of the metal ions. Because of the corrosive environment in the bath, iron dissolution is initiated, causing hydrogen evolution at the surface owing to the following reaction [1]

$$Fe(s) + 2H^+ \rightarrow Fe^{2+} + H_2(g) \qquad (1)$$
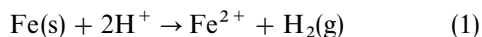
The accompanying change in pH alters the hydrolytic equilibrium which exists between the soluble primary phosphates and the insoluble tertiary phosphates of the heavy-metal ions present in the phosphatizing solution. This results in the conversion and deposition of insoluble heavy-metal tertiary phosphates. In a zinc–calcium-containing bath this chemical reaction results in the following reactions [1, 2]

$$3Zn^{2+} + 2H_2PO_4^- \leftrightarrow Zn_3(PO_4)_2 + 4H^+ \qquad (2)$$

$$3Ca^{2+} + 2H_2PO_4^- \leftrightarrow Ca_3(PO_4)_2 + 4H^+ \qquad (3)$$

$$Ca^{2+} + 2Zn^{2+} + 2H_2PO_4^- \rightarrow CaZn_2(PO_4)_2\downarrow + 4H^+ \qquad (4)$$

In this way a highly adherent phosphate coating can be deposited on the metal surface.

In the electrochemical phosphatizing process the specimen is used as the cathode. By using the specimen as a cathode in an electrolytic process an increase in pH at the surface can be achieved owing to the reduction of H^+ ions to $H_2(g)$

$$2H^+ + 2e^- \rightarrow H_2(g) \qquad (5)$$
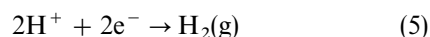
At the anode, water is decomposed and oxygen is generated

$$H_2O \rightarrow \tfrac{1}{2}O_2 + 2H^+ + 2e^- \qquad (6)$$
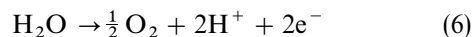
As a result of this pH increase in the vicinity of the cathode surface, the solute becomes supersaturated with phosphates which are then deposited at the cathode. This is due to the decreasing solubilities of phosphates with increasing pH.

In the present work, crystalline $Zn_3(PO_4)_2 \cdot 4H_2O$ (hopeite) and amorphous Zn–Ca phosphates with different Zn-to-Ca molar ratios were deposited by galvanostatic electrolysis with constant or pulsating current densities [6]. The electrolytes used were zinc–calcium phosphate solutions made acidic by the addition of nitric acid (pH 2). The products were analysed with respect to composition, structure, morphology and thermal characteristics.

2. Experimental procedure

Deposition of the amorphous phosphates were carried out at constant cathode current densities of 20–50 mA cm^{-2} in the temperature range 20–25 °C and with a duration of up to 3 min. The deposition of uniform crystalline $Zn_3(PO_4)_2 \cdot 4H_2O$ was performed with a pulsating cathode current density of 70 mA cm^{-2} (0.5 s with a 2 s pause) at 70 °C in periods up to 10 min. The electrolytes used were aqueous solutions of nitric acid (0.5–0.7 mol l^{-1}) saturated with tricalcium phosphate ($Ca_3(PO_4)_2$) and/or zinc phosphate dihydrate ($Zn_3(PO_4)_2 \cdot 2H_2O$), and with $Zn(NO_3)_2 \cdot 6H_2O$ (0–0.06 mol l^{-1}) added. A small amount of phosphoric acid was added in order to maintain a metal-to-phosphate molar ratio of 1.5. No other electrolytes were added. The electrolytes were stirred for 1 h to enhance the dissolution and mixing of the components. The pH values of the solutions were 2–2.3.

The anodes and cathode substrate were made of standard stainless steel (W. 1.4401). Other more corrosion-resistant anode and cathode materials can also be used. Before coating, the cathode specimens were cleaned carefully in a diluted 80 °C hot NaOH solution and afterwards in a 58 °C warm diluted sulphuric acid solution and then rinsed with distilled water. This was done to increase the adhesion of the coatings to the surface. After the coating formation the samples were rinsed with distilled water.

The resulting deposits on the cathode were examined as deposited after drying in air or as powders scraped from the cathode. For the examination a Philips PW 1050/25 X-ray diffractometer using Ni-filtered Cu Kα_1 radiation ($\lambda = 1.540\,51$ Å; 40 kV; 40 mA) and a Philips SEM 505 scanning electron microscope equipped with an EDAX 9000 for energy-dispersive X-ray analysis (EDXA) were used. For the thermal analysis (differential thermal analysis (DTA)-thermogravimetry (TG)) a Mettler TA1 thermal analyser was used. Surface area measurements were performed with a Micromeritics Instrument Corporation, Gemini 2375 Brunauer–Emmett–Teller (BET) surface area analyser.

3. Results and discussion

The amorphous phosphate composition is expressed as $Ca_{3-x}Zn_x(PO_4)_2 \cdot nH_2O$ but consists in fact of a mixture of different phosphates with variable solubilities: $Ca_5(PO_4)_3OH$ (hydroxyapatite), $CaHPO_4 \cdot 2H_2O$ (brushite), $CaHPO_4$ (monetite), $Ca_8H_2(PO_4)_6 \cdot 5H_2O$ (octacalcium phosphate) and β-$Ca_3(PO_4)_2$ (whitlockite), $CaZn_2(PO_4)_2$ (scholzite), $3Zn_3(PO_4)_2 \cdot Zn(OH)_2$ (zinc hydroxyapatite), $Zn_3(PO_4)_2 \cdot 4H_2O$ (hopeite), $ZnHPO_4 \cdot 3H_2O$, $ZnHPO_4 \cdot H_2O$, $Zn(H_2PO_4)_2 \cdot 2H_2O$ and $Zn(H_2PO_4)_2 \cdot 2H_3PO_4$.

By varying the zinc content in the electrolyte, the zinc content in the amorphous deposits (see Table II) varied within the range $x = 0$–1.5 for $Ca_{3-x}Zn_x(PO_4)_2 \cdot nH_2O$. The Zn-to-Ca molar ratios were determined by EDX.

Solution A (Table I) resulted after electrolysis in amorphous deposits with a Zn-to-Ca molar ratio of

1.0. The electrolysis was made at a constant cathodic current density of 30 mA cm^{-2} for 3 min on the stainless steel substrate. The large amount of zinc in the deposit compared with the content in the electrolyte was found to be caused by the existence of some zinc phosphates, with lower solubility than the calcium phosphates present in the solute. The zinc phosphates present in the solutions tend to precipitate in a larger amount than the calcium phosphates. The mass of phosphate deposited on the surface showed a nearly linear dependence on time in the range 0–40 g m^{-2} (Fig. 1). The EDX results of the Zn-to-Ca molar ratios for the other deposits are shown in Table II. The (Ca + Zn)-to-P molar ratios (Table II) were estimated by EDX to be slightly less than 1.5.

By applying higher constant current densities (much greater than 30 mA cm^{-2}) an increase in the pH gradient resulted in a large amount of non-uniform deposits with poor adhesion. Lower current densities (much less than 30 mA cm^{-2}) gave too small amounts of material deposited.

The crystalline $Zn_3(PO_4)_2 \cdot 4H_2O$ (hopeite) was deposited from solution D (Table I) at a pulsating cathode current density of 70 mA cm^{-2} (0.5 s with a 2 s pause) at 70 °C for times up to 10 min. The diffraction pattern (XRD) pattern of $Zn_3(PO_4)_2 \cdot 4H_2O$ (hopeite) removed from the cathode is shown in Fig. 2 together with reference data [7].

The adhesion of the pure calcium phosphate coating to the stainless steel substrate was of relatively poor quality but the adhesion increased with increasing zinc content in the coating. All the amorphous

TABLE I Contents of the electrolytes used for the electrolytic deposition of phosphates, with precipitates included

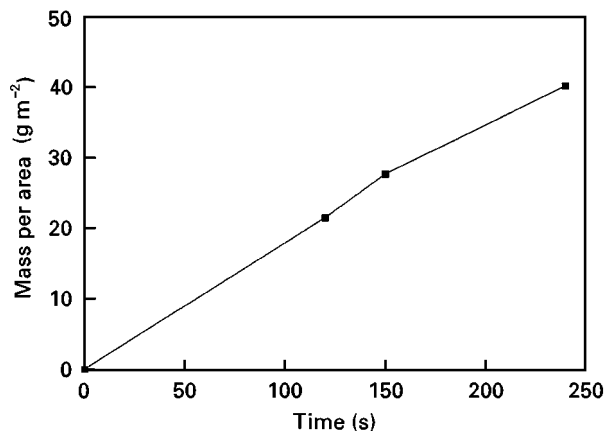| Solution	Ca^{2+} (mol l^{-1})	Zn^{2+} (mol l^{-1})	PO$_4^{3-}$ (mol l^{-1})	Zn-to-Ca ratio (mol mol^{-1})	NO$_{3-}$ (mol l^{-1})
A	0.43	0.06	0.33	0.14	0.61
B	0.43	0.03	0.31	0.07	0.61
C	0.43	–	0.28	–	0.61
D	–	0.31	0.28	–	0.61

Figure 1 Mass of amorphous phosphate deposited on the surface as a function of time, at room temperature and a constant cathodic current density of 30 mA cm^{-2}.

TABLE II Zn-to-Ca molar ratios in the deposits precipitated from solutions A, B and C at 25 °C for a constant cathodic current of 30 mA cm^{-2} for 3 min on stainless steel; the molar ratios were determined by EDX

Solution	Zn-to-Ca ratio (mol mol^{-1})	(Ca + Zn)-to-P ratio (mol mol^{-1})
A	1.0 ± 0.1	1.4 ± 0.1
B	0.5 ± 0.1	1.4 ± 0.1
C	0.0	1.4 ± 0.1
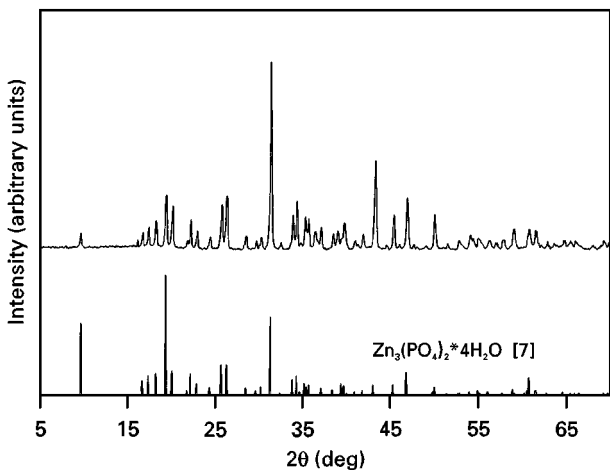
Figure 2 XRD pattern of $Zn_3(PO_4)_2 \cdot 4H_2O$ (hopeite) deposition layer (step scan; step size, 0.1 °C; 2 s per step).
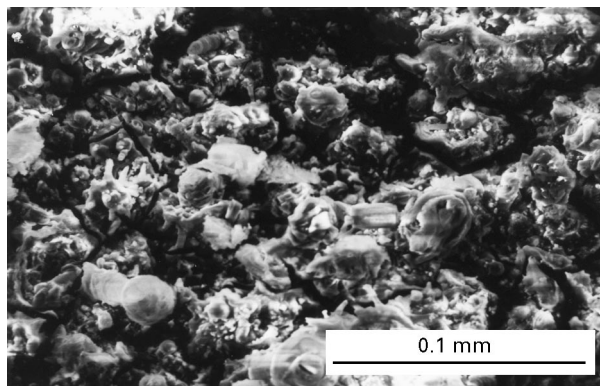

Figure 3 Scanning electron micrographs of amorphous Zn–Ca phosphate deposition layer (Zn-to-Ca molar ratio, 1.0).
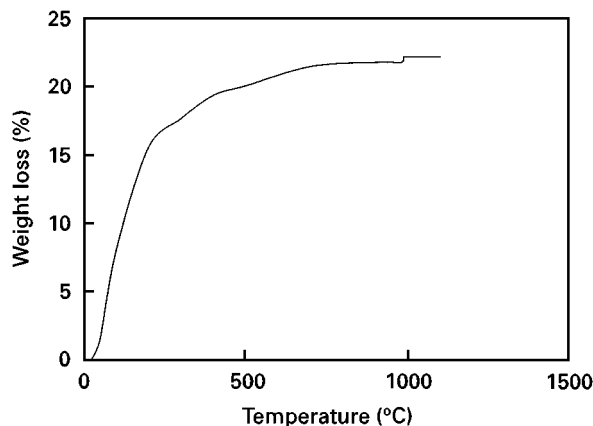

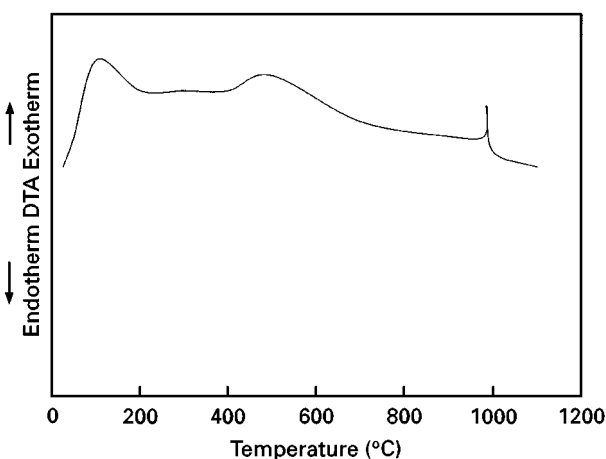Figure 4 Thermal analysis of amorphous Zn–Ca phosphates, (Zn-to-Ca molar ratio, 1.0; heating rate, 2 °C min^{-1}).

Figure 5 DTA of amorphous Zn–Ca phosphates (Zn-to-Ca molar ratio, 1.0; heating rate, 2 °C min^{-1}).

zinc–calcium phosphate coatings showed good adhesion to the substrate. The morphology of the amorphous phosphate deposited at 20 °C and with a constant cathodic current of 30 mA cm^{-2} for 3 min and with a Zn-to-Ca molar ratio of 1 was examined with the Philips SEM 505 scanning electron microscope. The deposit showed no uniform regularity (Fig. 3) but suggested a porous coating with relatively large surface area. BET multipoint surface area measurement showed a surface area of 28.4 m^2 g^{-1}.

The TG–DTA curves for the powder with a Zn-to-Ca molar ratio of 1 is shown in Figs 4 and 5. The analyses were carried out in dry air with a heating rate of 2 °C min^{-1}. The crucible was made of platinum and the DTA reference substance was Al_2O_3.

The TG curve in Fig. 4 shows a weight loss of 15 wt% up to 200 °C which is caused by the liberation of large amounts of adsorbed H_2O. Weight losses up to 600 °C are due to the liberation of adsorbed H_2O and the reactions

$$2HPO_4^{2-} \rightarrow P_2O_7^{4-} + H_2O\uparrow \tag{7}$$

$$PO_4^{3-} + H_2O(\text{lattice}) \rightarrow HPO_4^{2-} + OH^- \tag{8}$$

$$2HPO_4^{2-} + 2OH^- \rightarrow P_2O_7^{4-} + H_2O\uparrow + 2OH^- \tag{9}$$

The weight losses from 600 to 900 °C may be caused by the reaction following Equation 9, i.e.

$$P_2O_7^{4-} + 2OH^- \rightarrow 2PO_4^{3-} + H_2O\uparrow \tag{10}$$

which results in the formation of crystalline PO_4^{3-}-containing phosphates. At 980 °C the powder melts. The DTA curve in Fig. 5 shows only the endothermic reactions caused by the water removal and no signs of exothermic crystallization. Different forms of crystallinity were determined by XRD on powders removed from the cathode and calcinated in a platinum crucible at different temperatures (500, 600, 750 and 900 °C). Fig. 6 shows the XRD patterns (step scan; step size, 0.1 °C; 2 s per step) of the powder with a Zn-to-Ca molar ratio of 1 heated at 3 °C min^{-1} and calcinated for 1 h at different temperatures in an oven.
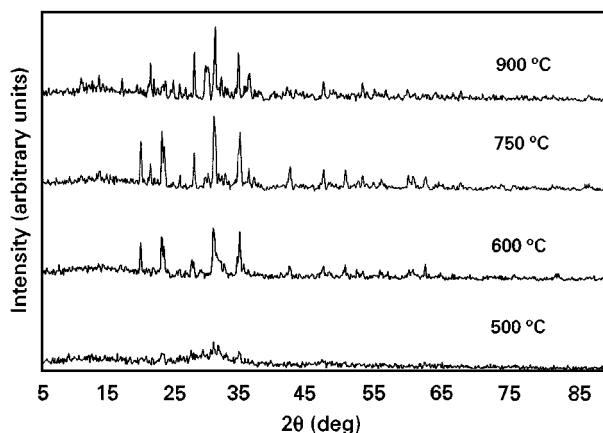
Figure 6 XRD powder diffraction patterns of Zn-to-Ca phosphate molar ratio 1.0 as a function of heat treatment (step scan; step size, 0.1 °C; 2 s per step).
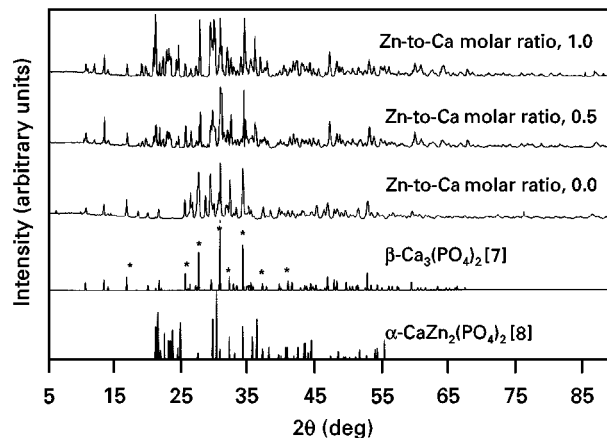

Figure 7 XRD powder diffraction patterns of Zn–Ca phosphates as a function of molar ratio. Samples calcinated at 900 °C for 1 h (step scan; step size, 0.1 °C; 25 s per step).

At 500 °C, the powder is still amorphous but, at 600 °C, one or more unidentified crystalline phases begin to appear. At 900 °C, the first-formed phases are changed to other phases, perhaps owing to Equation 10.

Powders with different Zn-to-Ca ratios were removed from the cathodes and heated at 1.8 °C min^{-1} to 900 °C where they were calcinated for 1 h. The calcium phosphate powder (Zn-to-Ca ratio of 0 (Fig. 7)) was, after calcination, identified by XRD as β-$Ca_3(PO_4)_2$ (whitlockite) with a rhombohedral structure (space group, $R3c$) [7]. The powders with zinc content resulted in a two-phase system of crystalline solids. Solid solutions $Zn_3(PO_4)_2$ in β-$Ca_3(PO_4)_2$ (whitlockite) were identified together with reflections from α-$CaZn_2(PO_4)$. The XRD patterns of the crystalline phosphates are shown in Fig. 7. The reflections from β-$Ca_3(PO_4)_2$ in the two-phase system of crystalline Zn–Ca phosphates had some slightly different positions compared with the reflections from the pure β-$Ca_3(PO_4)_2$ owing to a solid solution of $Zn_3(PO_4)_2$.

The unit-cell dimensions for the rhombohedral $R3c$ whitlockite phase present in all the calcinated powders were calculated by the method of least squares. The dimensions for the pure β-$Ca_3(PO_4)_2$ were $a = 10.412 \pm 0.004$ Å and $c = 37.487 \pm 0.049$ Å. The zinc-containing two-phase powders gave slightly different unit-cell dimensions for the β-$Ca_3(PO_4)_2$ phase present. The reflections assumed to be from β-$Ca_3(PO_4)_2$ were used for the unit-cell calculation of the pure β-$Ca_3(PO_4)_2$ powder. The reflections used for the calculation are indicated with an asterisk in Fig. 7. All unit-cell parameters calculated for the β-$Ca_3(PO_4)_2$ phases are shown in Table III. The differences in the unit-cell parameters for the β-$Ca_3(PO_4)_2$ phases were assumed to be caused by the substitution of some Ca^{2+} ions in the β-$Ca_3(PO_4)_2$ phase with Zn^{2+} giving solid solutions of $Zn_3(PO_4)_2$ in β-$Ca_3(PO_4)_2$. The solid solutions are expressed as $Ca_{3-x}Zn_x(PO_4)_2$ phases with β-$Ca_3(PO_4)_2$ structure.

Kreidler and Hummel [8] have extensively studied the system $Ca_3(PO_4)_2$–$Zn_3(PO_4)_2$ and it was found that β-$Ca_3(PO_4)_2$ can take up to 10.6 mol% $Zn_3(PO_4)_2$ into solid solution at 1000 °C. The amount of $Zn_3(PO_4)_2$ in solution was determined by the posi-

TABLE III Unit-cell parameters of solid solutions of $Zn_3(PO_4)_2$ in β-$Ca_3(PO_4)_2$ (whitlockite) with a β-$Ca_3(PO_4)_2$ structure

Zn-to-Ca ratio in mixed-phase powders (mol mol^{-1})	a (Å)	c (Å)
Whitlockite [7]	10.428 ± 0.001	37.404 ± 0.006
0.0	10.412 ± 0.004	37.487 ± 0.049
0.5	10.362 ± 0.005	37.363 ± 0.033
1.0	10.331 ± 0.006	37.437 ± 0.045

tion of the 46.9° (2θ) pure β-$Ca_3(PO_4)_2$ peak compared with the peak position for known solid solutions. The peak position showed a linear dependence on $Zn_3(PO_4)_2$ in solid solution. Kreidler and Hummel [8] found that, at the solid solution limit of 10.6 mol% at 1000 °C, the 46.9° (2θ) peak had changed to 47.35° (2θ).

In our case the peak position has changed from 46.9° to 47.30° which, according to Kreidler and Hummel [8], results in a solid solution of 9 mol% $Zn_3(PO_4)_2$ in β-$Ca_3(PO_4)_2$ at 900 °C. The existence of α-$CaZn_2(PO_4)$ together with the solid solution of $Zn_3(PO_4)_2$ in β-$Ca_3(PO_4)_2$ in β-$Ca_3(PO_4)_2$ fully agrees with the phases determined by Kreidler and Hummel [8].

4. Conclusions

Electrolytic depositions of amorphous Zn–Ca phosphates with various Zn-to-Ca molar ratios and crystalline $Zn_3(PO_4)_2 \cdot 4H_2O$ (hopeite) were accomplished on stainless steel by electrolysis of solutions of Zn–Ca phosphates acidified with nitric acid. The deposition occured as a result of an electrolytically induced pH gradient in the vicinity of the cathode substrate surface.

The deposition of the amorphous phosphates was performed at 20–25 °C and at constant cathode currents of 20–50 mA cm^{-2}. The deposits contained up to 20 wt% water. The amount deposited showed a nearly linear dependence with time in the range 0–40 g m^{-2} at a constant cathode current of 30 mA cm^{-2}.

The deposits showed no uniform regularity in morphology and showed a porous coating with a relatively large surface area. Surface areas of the amorphous deposits were of the order of 28 m^2 g^{-1}. Crystallization of the amorphous deposits occured at 500–600 °C, resulting in β-$Ca_3(PO_4)_2$ at 900 °C for the Ca-containing deposits and a two-phase system with $Ca_{3-x}Zn_x(PO_4)_2$ and α-$CaZn_2(PO_4)$ for the Zn–Ca phosphates.

The deposition of the crystalline $Zn_3(PO_4)_2 \cdot 4H_2O$ (hopeite) occurred for a 0.5 s pulsating cathode current density of 70 mA cm^{-2} followed by a 2 s pause at 70 °C for periods of less than 10 min.

Acknowledgement

References

1. W. RAUSCH, "Die Phosphatierung von Metallen" (Leuze, 1974).
2. D. B. FREEMAN, "Phosphating and metal pre-treatment" (Woodhead–Faulkner, 1986).
3. M. SHIRKHANZADEH, *Mater. Lett.* **14** (1992) 27.
4. H. MONMA, *J. Mater. Sci.* **29** (1994) 949.
5. T. V. VIJAYARAGHAVAN and A. BENSALEM, *J. Mater. Sci. Lett.* **13** (1994) 1782.
6. T. STEENBERG, E. CHRISTENSEN and N. J. BJERRUM, Danish Patent Appl. 0910/96 (1996).
7. Joint Committe on Powder Diffraction Standards, "Powder diffraction file" (International Center for Diffraction Data, Swarthmore, PA, 1995) PDF-2 Database Sets 1–45.
8. E. R. KREIDLER and F. A. HUMMEL, *Inorg. Chem.* **6** (1967) 526.